Low-temperature orientation dependence of step stiffness on {111} surfaces

T. J. Stasevich,* Hailu Gebremariam, and T. L. Einstein[†]

Department of Physics, University of Maryland, College Park, Maryland 20742-4111, USA

M. Giesen, C. Steimer, and H. Ibach

Institut für Schichten und Grenzflächen (ISG), Forschungszentrum Jülich, D-52425 Jülich, Germany

(Received 19 November 2004; published 23 June 2005)

For hexagonal nets, descriptive of {111} fcc surfaces, we derive from combinatoric arguments a simple, low-temperature formula for the orientation dependence of the surface step line tension and stiffness, as well as the leading correction, based on the Ising model with nearest-neighbor (NN) interactions. Our formula agrees well with experimental data for both Ag and Cu{111} surfaces, indicating that NN interactions alone can account for the data in these cases (in contrast to results for Cu{001}). Experimentally significant corollaries of the low-temperature derivation show that the step line tension cannot be extracted from the stiffness and that with plausible assumptions the low-temperature stiffness should have six-fold symmetry, in contrast to the three fold symmetry of the crystal shape. We examine Zia's exact implicit solution in detail, using numerical methods for general orientations and deriving many analytic results including explicit solutions in the two high-symmetry directions. From these exact results we rederive our simple result and explore subtle behavior near close-packed directions. To account for the three-fold symmetry in a lattice gas model, we invoke an orientation-dependent trio interaction and examine its consequences.

I. INTRODUCTION

Most of our current understanding of surface morphology is based on the step-continuum model,[1] which treats the step itself as the fundamental unit controlling the evolution of a surface. In this model, the step stiffness $\tilde{\beta}$ serves as one of the three fundamental parameters; it gauges the "resistance" of the step to meandering and ultimately accounts for the inertia of the step in the face of driving forces. The stiffness can be derived from the step line tension $\beta(\theta)$, the excess free energy per length associated with a step edge of a specified azimuthal orientation θ. From β, the two-dimensional equilibrium crystal shape (i.e., the shape of the islands) is determined.

The goal of this paper is to find low-temperature (T) formulas for $\beta(\theta)$ and thence $\tilde{\beta}(\theta) \equiv \beta(\theta) + \beta''(\theta)$ as functions of the azimuthal misorientation θ, assuming just nearest-neighbor interactions in plane and an underlying {111} surface. Such surfaces are characterized by a sixfold symmetric triangular (hexagonal) lattice, allowing all calculations to be done in the first sextant alone (from 0° to 60°). In contrast to $\beta(\theta)$, we shall find that at low T, $\tilde{\beta}(\theta)$ is insensitive, under plausible assumptions, to the symmetry breaking by the second substrate layer, so that plots from 0° to 30° suffice. Although an analytic solution exists for the orientation dependence of $\beta(\theta)$ on a square lattice,[2–4] only an implicit solution to a sixth-order equation has been found for a hexagonal lattice.[5] This makes comparisons to experiment rather arduous, particularly when trying to compare data on $\tilde{\beta}(\theta)$, which is related to $\beta(\theta)$ through a double derivative with respect to θ. Fortunately, we will see that a remarkably simple formula exists for the orientation dependence of $\tilde{\beta}$ at temperatures which are low compared to the characteristic energy of step fluctuations (i.e., the kink energy or the energy per length along the step). For noble metals, room temperature lies in this limit, facilitating direct comparisons to experiment.

Motivating this work is a recent finding[6] that the square-lattice nearest-neighbor (NN) Ising model underestimates $\tilde{\beta}$ by a factor of 4 away from close-packed directions on Cu{001}. Later work[7–9] showed that much (but not all) of this discrepancy could be understood by considering the addition of next-nearest-neighbor (NNN) interactions. For the triangular lattice, we will see that such a longer-range interaction is not required to describe the orientation dependence of $\tilde{\beta}$.

In the following section, we characterize steps on a hexagonal lattice and perform a low-temperature expansion of the lattice-gas partition function, assuming only NN bonds are relevant, and derive both $\beta(\theta)$ and $\tilde{\beta}(\theta)$. We obtain a remarkably simple expression for the latter in Eq. (18). Since this low-T limit is determined by geometric-configurational considerations, it becomes problematic near close-packed orientations ($\theta=0°$), where the kinks must be thermally activated. Therefore, we make use of exact results to assess in several ways how small θ can be before the simple expression becomes unreliable. In Sec. III, we present three general results for island stiffness that are valid in the experimentally relevant low-T limit when configurational considerations dominate the thermodynamics. We show that the line tension cannot be [re]generated from the stiffness and that the stiffness can have full six-fold symmetry even though the substrate and the line tension have just three-fold symmetry. Accounting for such three-fold symmetry with a lattice-gas model on a hexagonal grid requires an extension from the conventional parametrization; we posit *orientation-dependent* interactions between three atoms at the apexes of an equilateral triangle with NN legs. In Sec. IV, we compare our results to experiments on Ag and Cu{111} surfaces,
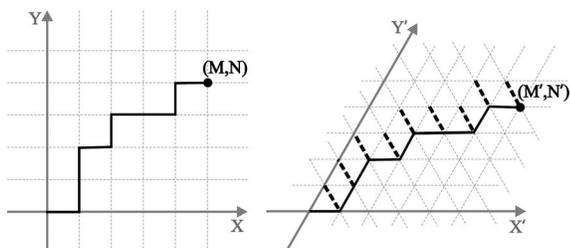
FIG. 1. There is a one-to-one correspondence between the shortest-distance steps connecting points on a square lattice [(a), left panel] and the shortest distance steps connecting points on a triangular lattice [(b), right panel]. This figure shows two corresponding steps. Analogous to the $M+N$ broken bonds oriented at 0° and 90° on a square lattice, there are $M'+N'$ broken bonds oriented at 0° and at 60° on a triangular lattice. However, there are another $M'+N'$ broken bonds oriented at 120° on a triangular lattice [drawn as bold dashed lines].

showing that Eq. (18) provides a good approximation and, thus, that NNN interactions are much less important than on Cu{001}. The final section offers a concluding discussion. Three appendixes give detailed calculations of the leading correction of the low-T expansion, of explicit analytic and numerical results based on Zia's exact implicit solution,[5] and of Eq. (18) as the low-T limit of Zia's solution.

II. ISING EXPANSION ON A TRIANGULAR LATTICE

A. Recap of results for square lattice

The orientation dependence of β on {111} surfaces can be determined by first calculating the free energy F of a single step oriented at a fixed angle θ. To approximate this, we perform a low-temperature Ising expansion of the partition function, similar to the one used by Rottman and Wortis.[3] They considered a step on a square lattice with one end fixed to the origin and the other end, a distance L away, fixed to the point ($M \equiv L \cos \theta$, $N \equiv L \sin \theta$). Such a step is shown in Fig. 1(a). The single-layer island (or compact adatom-filled region) is in the lower region, separated by the step edge—which is drawn as a bold solid line—from the upper part of the figure, representing the "plain" region. They found the step energies associated with the broken bonds of the step-edge to be

$$E_n = \varepsilon(M + N + 2n), \quad n = 0,1,2,\ldots, \quad (1)$$

where ε, sometimes[10] called the "Ising parameter," is the bonding energy associated with the "severed half" of the NN lattice-gas bond. Since the NN lattice-gas energy ϵ_1 is attractive (negative), and half of it is attributed to the atom on each end, it "costs" a positive energy $\varepsilon = -\frac{1}{2}\epsilon_1$ for each step-edge atom. Because longer steps require more step-edge atoms, the step energy is only a function of the step length, $M+N+2n$. Thus, E_0 corresponds to the shortest possible step. To increase the length of this step, two more step-edge links—corresponding to one more step-edge atom—must be added, one going away from the fixed endpoint and one going toward it. Because this corresponds to two more broken bonds, in general, $E_{n+1} - E_n \equiv \Delta E = 2\varepsilon$. With these energies, we can

write down the partition function Z_θ, assuming θ is fixed but L is large enough so that integer values of M and N can be found,

$$Z_\theta = g_{M,N}(0)e^{-E_0/kT} + g_{M,N}(1)e^{-E_1/kT} + \cdots, \quad (2)$$

where $g_{M,N}(n)$ corresponds to the number of ways a step of length $M+N+2n$ can be arranged between the two endpoints.

For low temperatures, only the first term in Eq. (2) need be considered [Appendix A provides the leading correction term, which gives a correction of order $\exp(-2\varepsilon/k_B T)$]. To lowest order, then, F is

$$F \approx E_0 - k_B T \ln\binom{M+N}{M}, \quad (3)$$

where we have inserted the value of $g_{M,N}(0)$ obtained from a simple combinatorial analysis.[3,11] After taking the thermodynamic limit ($M, N \gg 1$) and using Stirling's approximation, F becomes

$$F \approx E_0 - k_B T[(M+N)\ln(M+N) - M \ln M - N \ln N]. \quad (4)$$

B. Triangular lattice step energy

In order to extend this result to a step on a triangular lattice, we need to make a few minor adjustments. First, we introduce a linear operator $\mathcal{L}$ that transforms the coordinates of a point on a square lattice (M,N) to those on a triangular lattice (M',N'); cf. Fig. 1(b). This operator finds the position of a point in a coordinate system whose positive y axis is bent at 60° with respect to the positive x axis,

$$\binom{M'}{N'} = \mathcal{L}\binom{M}{N} = \begin{pmatrix} 1 & -1/\sqrt{3} \\ 0 & 2/\sqrt{3} \end{pmatrix}\binom{M}{N}. \quad (5)$$

With the aid of $\mathcal{L}$, we can see how E_0 changes on a triangular lattice. To begin, we imagine a step in the first sextant (from 0° to 60° degrees in the plane) starting at (0,0) and ending at (M',N'). Such a step is shown in Fig. 1(b). As before, the bold solid line represents the step edge with the bottom region a layer higher than the top (or, alternatively phrased, it separates the upper, adatom-free region from the lower, adatom-filled region). The broken bonds required to form the step will have only three orientations, 0°, 60°, and 120°. If we consider the shortest step between the two points (corresponding to energy E_0), then there will be exactly $M'+N'$ broken bonds oriented at 0° and 60° (these bonds are analogous to those oriented at 0° and 90° on a square lattice). There will be another $M'+N'$ broken bonds oriented at 120° (drawn as bold, dashed lines in Fig. 1). In total, there will be $2(M'+N')$ broken bonds. Since ε is the energy of these severed bonds, $E_0^\Delta = 2\varepsilon(M'+N')$. Thus, the energy is proportional to the step length, as was the case on a square lattice. Using $\mathcal{L}$ to write M' and N' in terms of M and N gives

$$E_0^\Delta = 2\varepsilon\left(M + \frac{N}{\sqrt{3}}\right) = 2\varepsilon L\left(\cos\theta + \frac{\sin\theta}{\sqrt{3}}\right). \quad (6)$$

C. Triangular lattice step degeneracy

Next we consider the degeneracy factors $g^\Delta(n)$ on a triangular lattice. For the ground state $g^\Delta(0)$ there is a one-to-one correspondence between the shortest distance steps connecting two points on a square lattice and the corresponding steps on a triangular lattice (see Fig. 1). Therefore, we know that the degeneracy factor $g^\Delta_{M',N'}(0)$ for steps of energy E_0^Δ on a triangular lattice must be identical to $g_{M',N'}(0)$ implicit in Eq. (3). More precisely, if we assume the point (M,N) is in the first quadrant, and (M',N') is in the first sextant, then on a square lattice, shortest-distance step-links are oriented at either 0° or 90°, whereas on a triangular lattice they are oriented at either 0° or 60° (i.e., in the first sextant, the shortest path cannot have links oriented at 120°). In both cases, the individual step-links can only be oriented in one of two directions and, therefore, besides the transformation between coordinates, the total number of path arrangements is the same.

Using Eq. (3) and Stirling's approximation, we find the low-temperature free energy (Appendix A provides the lowest-order correction),

$$F \approx E_0^\Delta - k_B T \ln[g_{M',N'}(0)] \approx E_0^\Delta - k_B T[(M' + N')\ln(M' + N') - M' \ln M' - N' \ln N'].$$
(7)

Alternatively, we can transform Eq. (4) for the square lattice to the triangular lattice by just replacing $N/M \equiv \tan\theta$ with $(2\tan\theta)/(\sqrt{3} - \tan\theta)$. (This ratio is just N'/M', so it might be termed $\tan\theta'$.) [We must also make a simple (and ultimately inconsequential) change to E_0.]

We now take the thermodynamic limit $(M',N' \gg 1)$ and write M' and N' in terms of $M \equiv L\cos\theta$ and $N \equiv L\sin\theta$ via Eq. (5). Then dividing by L and defining[12]

$$\eta_\pm(\theta) = \cos\theta \pm \frac{\sin\theta}{\sqrt{3}}, \quad \eta_0(\theta) = \frac{2}{\sqrt{3}}\sin\theta,$$
(8)

all non-negative in the first sextant, we straightforwardly find the step-edge line tension (or free energy per unit length[13]) $\beta(\theta)$,

$$a_\parallel \beta(\theta) = 2\varepsilon \eta_+(\theta) - k_B T[s_+(\theta) - s_-(\theta) - s_0(\theta)],$$
(9)

where $a_\parallel$ is the nearest-neighbor spacing and

$$s_i(\theta) = \eta_i(\theta)\ln \eta_i(\theta), \quad i = +,0,-.$$
(10)

For the special case of the maximally kinked orientation, Eqs. (8)–(10) reduce to

$$a_k\beta(30°) = 2\varepsilon - k_B T \ln 2,$$
(11)

where $a_k = (\sqrt{3}/2)a_\parallel$ for the {111} surface. This result for the maximally kinked case (including steps at $\theta = 45°$ on a square lattice) was derived earlier from a direct examination of entropy.[14]

For specificity, we recall some established results. For a hexagonal lattice with just nearest-neighbor attractions, the critical temperature T_c is long known,[15]

$$k_B T_c = 2\varepsilon/\ln 3 \approx 1.82\varepsilon.$$
(12)

From the equilibrium shape of islands over a broad temperature range, Giesen *et al.*[10] deduced that the free energy per lattice spacing in the maximally kinked directions is 0.27 ± 0.03 eV on Cu{111} and slightly smaller, 0.25 ± 0.03 eV, on Ag{111}. Combining these results with Eq. (11), we find ε is 0.126 eV on Cu{111} and 0.117 eV on Ag{111}. In both cases, then, room temperature is somewhere between $T_c/9$ and $T_c/8$.

D. Main result: Simple expression for low-T stiffness

As shown just above, the step stiffness $\tilde\beta = \beta(\theta) + \beta''(\theta)$ computed from Eq. (9) depends to leading order only on the combinatoric entropy terms s_0 and $s_\pm$ of Eqs. (9) and (10). Hence,

$$\frac{d^2 s_i}{d\theta^2} \equiv s_i'' = -\eta_i \ln \eta_i + \frac{\eta_i'^2 - \eta_i^2}{\eta_i},$$
(13)

so that[16]

$$\tilde s_i \equiv s_i + s_i'' = \frac{\eta_i'^2 - \eta_i^2}{\eta_i}.$$
(14)

With this notation, the reduced stiffness is

$$\frac{\tilde\beta a_\parallel}{k_B T} = \tilde s_0 + \tilde s_- - \tilde s_+,$$
(15)

where

$$\tilde s_0 = \frac{2}{\sqrt{3}}\frac{\cos 2\theta}{\sin\theta},$$
(16)

$$\tilde s_\pm = \frac{-2\cos 2\theta \mp 2\sqrt{3}\sin 2\theta}{3\cos\theta \pm \sqrt{3}\sin\theta}.$$
(17)

Adding these terms together gives our *main* result—a remarkably simple form for the reduced stiffness in the low-temperature $(T \ll \varepsilon/k_B)$ limit,

$$\frac{k_B T}{\tilde\beta a_\parallel} = \frac{\sin(3\theta)}{2\sqrt{3}} = \frac{3m - m^3}{2\sqrt{3}(1 + m^2)^{3/2}},$$
(18)

where $m = \tan\theta$.

E. Synopsis of exact results and application to range of breakdown of low-T limit near $\theta = 0$

To test how low the temperature should be for Eq. (18) to be a good approximation, we compare it to a numerical evaluation of the exact implicit solution of the Ising model. The derivation of this solution, outlined by Zia,[5] gives a sixth order equation for $\beta(\theta)$. In essence, after conversion to our notation, his key result for the step free energy β is given by[17]

$$\frac{\beta a_\parallel}{k_B T} = \eta_0(\theta)\psi_1(\theta, T/T_c) + \eta_-(\theta)\psi_2(\theta, T/T_c),$$
(19)

where the ψ's are the solutions of the pair of simultaneous equations for the angular constraint,

$$\frac{\sinh\psi_2 - \sinh(\psi_1 - \psi_2)}{\sinh\psi_1 + \sinh(\psi_1 - \psi_2)} = \frac{\eta_-}{\eta_0} = \frac{\sqrt{3}\cot\theta - 1}{2}, \quad (20)$$

and the thermal constraint,

$$\cosh\psi_1 + \cosh\psi_2 + \cosh(\psi_1 - \psi_2) = f(z) \equiv \frac{1 + 3z^2}{2(z - z^2)}, \quad (21)$$

where $z \equiv \exp(-2\varepsilon/k_BT) = 3^{-T_c/T}$, via Eq. (12). The ratio η_-/η_0 of Eq. (20) is a monotonically decreasing function which is ∞ at $\theta = 0°$, 1 at $\theta = 30°$, and 0 at $\theta = 60°$.

In these high-symmetry directions, Eqs. (20) and (21) yield analytic solutions for β and $\tilde{\beta}$,

$$\frac{\beta(0)a_\parallel}{k_BT} = 2\cosh^{-1}\left(\frac{-1 + \sqrt{3 + 2f}}{2}\right), \quad (22)$$

$$\frac{\tilde{\beta}(0)a_\parallel}{k_BT} = \frac{2}{3}\frac{\sqrt{2(3 + 2f)(f - \sqrt{3 + 2f})}}{\sqrt{3 + 2f} - 1}, \quad (23)$$

$$\frac{\beta(\pi/6)a_\parallel}{k_BT} = \frac{2}{\sqrt{3}}\cosh^{-1}\left(\frac{f - 1}{2}\right), \quad (24)$$

$$\frac{\tilde{\beta}(\pi/6)a_\parallel}{k_BT} = \frac{2\sqrt{3(f - 3)(f + 1)}}{f + 3}. \quad (25)$$

Details are provided in Appendix B. Akutsu and Akutsu[18] also derived these equations, in different notation[19] and from the more formal perspective of the imaginary path-weight method. Symmetry dictates that the solution at $\theta = 60° = \pi/3$ is the same solution as that at $\theta = 0°$. Furthermore, at $T = T_c$, $f(z) = 3$, so Eqs. (22)–(25) all go to 0, as expected.

To find $\tilde{\beta}$ in general directions, we solve Eqs. (20) and (21) [or, equivalently, Eq. (B4)] numerically. As Fig. 2 shows, once T decreases to nearly $T_c/9$, Eq. (18) more or less coincides with the exact numerical solution for the stiffness. At such low temperatures (compared to T_c), the approximation only fails below some very small, temperature-sensitive critical angle θ_c. Although it might seem easy to determine this angle by eye, estimating it quantitatively turns out to be a subtle and somewhat ambiguous task. We discuss two possible estimation techniques below.

In the first approach, we estimate θ_c to be the angle θ_1 at which the *curvature* of the exact solution changes sign. The points on the solid curve in Fig. 3 show θ_1 at several temperatures ranging from $T_c/9$ to $T_c/4$. At temperatures near and above $T_c/4$, θ_1 does not reliably estimate θ_c because there is a sizable curvature-independent difference between the exact solution and the approximation given in Eq. (18) evident even at $\theta = 30°$ (see Fig. 2). On the other hand, as the temperature dips below $T_c/5$, this difference fades, and the use of θ_1 to estimate θ_c becomes ever more precise.

A second, more fundamental way to estimate θ_c comes from an examination of the assumptions required to derive the simple expression for the low-T limit Eq. (18) directly
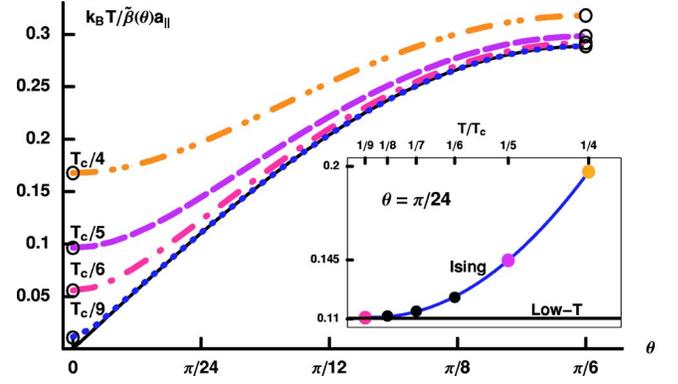

FIG. 2. (Color online) As the temperature drops close to $T_c/9$ (just below room temperature for Cu and Ag{111} surfaces), the numerical evaluation of the exact stiffness (Ref. 5) approaches the solid line representing the low-temperature approximation given in Eq. (18). The small circles indicate evaluations using the exact results of Eqs. (23) and (25). At $T_c/9$, when θ decreases, the exact solution begins to deviate from the approximation when its curvature changes sign near $\theta \approx \pi/100 = 1.8°$. The scale here is linear, in contrast to the logarithmic scale of Fig. 2 of Ref. 6. The inset shows more fully how the exact stiffness approaches the low-temperature limit for the particular azimuthal angle $\theta = \pi/24 = 7.5°$.

from the exact solutions Eqs. (20) and (21). In Appendix C we show that to do so θ must be greater than some θ_2 satisfying

$$\cot\theta_2 \ll \left(\frac{4f - 1}{\sqrt{3}}\right). \quad (26)$$

To give definite meaning to this inequality, we estimate θ_c directly from Fig. 2 at a single temperature, say $T_c/5$. At that temperature, θ_c is nearly 10°. If θ_2 is to accurately represent
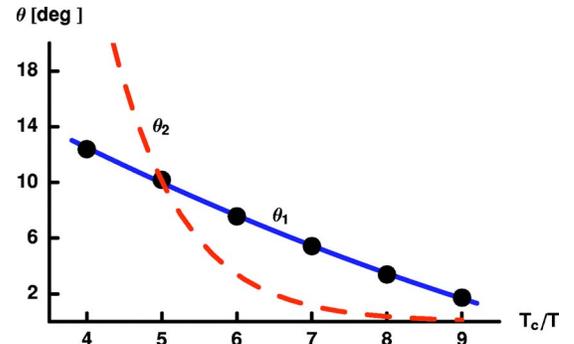

FIG. 3. (Color online) Two estimates for the critical angle θ_c, below which the approximation given in Eq. (18) begins to fail, as a function of T_c/T. The black dots connected by the solid, blue line represent the first estimate, defined to be the angle θ_1 at which the curvature of the numerically determined inverse stiffness changes sign. The dashed, red line represents the second estimate, $\theta_2 = \cot^{-1}[(4f - 1)/(50\sqrt{3})]$. At angles below θ_c, the three theorems of Sec. III break down, and higher order terms are required in the expansion of the step partition function. At temperatures between $T_c/9$ and $T_c/8$ (roughly room temperature for Cu and Ag{111} surfaces), θ_c is on the order of a few degrees.
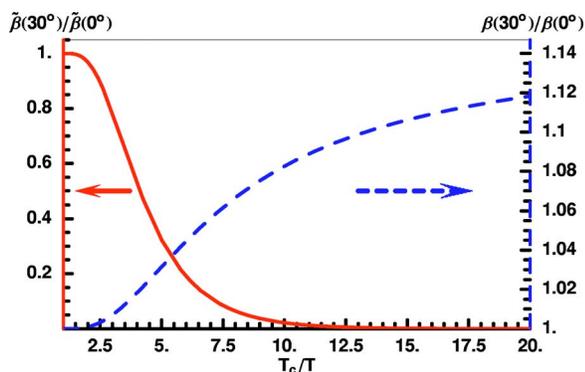
FIG. 4. (Color online) Ratio of the stiffness (solid red curve, left ordinate) and the free energy per length (dashed blue curve, right ordinate) for edges oriented in the maximally zig-zagged ($\theta=30°$) and close-packed ($\theta=0°$) directions, based on taking the ratios of Eqs. (25) and (23) and of Eqs. (24) and (22), respectively. The line-tension ratio increases slowly but monotonically to the $T=0$ limit $2/\sqrt{3}\approx 1.15$. In contrast, the stiffness ratio plummets toward 0, the value predicted by Eq. (18), providing an indicator how low T must be for this simple low-T formula to be a good approximation at all angles.

θ_c, it should also be around $10°$ at $T_c/5$. We enforce this by interpreting the $\ll$ in Eq. (26) to mean $=1/50$. The dashed (red online) curve in Fig. 3 shows the resulting θ_2 as a function of temperature. Clearly θ_1 and θ_2 are very different estimates for θ_c. While θ_2 is reliable at all temperatures (unlike θ_1), it is less precise than θ_1 at lower temperatures. A combination of θ_1 and θ_2 is therefore the best estimate for θ_c, being closer to θ_1 at lower temperatures, and closer to θ_2 at higher temperatures.

In essence, θ_c is no more than a few degrees between $T_c/9$ and $T_c/8$, regardless of which estimation technique is used. We therefore reach the practical conclusion that Eq. (18) is valid for almost all angles at temperatures near and below $T_c/8$, which fortunately happens to be around room temperature for Cu and Ag{111}.

Finally, we emphasize that $\widetilde{\beta}$ varies significantly with angle, especially at lower temperatures [where the equilibrium crystal shape (ECS) is hexagonal rather than circular]. If one wants to approximate $\widetilde{\beta}$ as isotropic rather than using Eq. (18), one should not pick its value in the close-packed direction (viz. $\theta=0°$); Fig. 4 provides stunning evidence of this conclusion. From Eq. (18) we also see that at low-temperatures the stiffness actually *increases* linearly with temperature. This contrasts with its behavior at high temperatures, where $\widetilde{\beta}$ must ultimately decrease as the ECS becomes more nearly circular and the steps fluctuate more easily.

III. GENERAL RESULTS FOR STIFFNESS IN LATTICE-GAS MODELS IN LOW-TEMPERATURE APPROXIMATION

In this section we present three "theorems" that are valid under two conditions: First, the energy term in the free energy must be a linear combination of $\cos\theta$ and $\sin\theta$. From

Eq. (6) and (implicitly) Eq. (3) we see that this property holds true in general for lattice-gas models, even when considering next-nearest neighbors and beyond.[20] Second, the temperature must be low enough so that the entropy is adequately approximated by the contribution of the lowest order term, $k_B \ln g(0)$. This entropic contribution is due exclusively to geometry or combinatorics of arranging the fixed number of kinks forced by azimuthal misorientation. Hence, it must vanish near close-packed directions ($0°$ and $60°$ in the first sextant). For angles sufficiently close to these directions, in our case less than θ_c, the leading term becomes dominated by higher-order terms, and the three results no longer apply.

A. No contribution from energy to lowest-order stiffness (LOS)

The first theorem is a remarkable consequence of the first condition, that the energy term in the free energy is a linear combination of $\cos\theta$ and $\sin\theta$. Since the stiffness $\widetilde{\beta}(\theta) \equiv \beta(\theta)+\beta''(\theta)$ and since $\cos''\theta=-\cos\theta$ and $\sin''\theta=-\sin\theta$, we see that *the lattice-gas energy makes no contribution whatsoever to the low-T limit of reduced stiffness*, as shown explicitly for square lattices long ago.[3,11] Thus, we retrieve the result that the leading term in a low-temperature expansion of the reduced stiffness $\widetilde{\beta}(\theta)/k_B T$ depends only on $g(0)$, which is determined solely by geometric (combinatoric) properties. Of course, higher-order terms (which are crucial near close-packed directions) do have weightings of the various configurations that depend on Boltzmann factors involving the characteristic lattice-gas energies. Furthermore, next-nearest-neighbor interactions can (at least partially) lift the $g(0)$-fold degeneracy of the lowest energy paths.[9]

B. Step line tension not extractable from LOS

An important corollary is that from the stiffness it is impossible to retrieve the energetic part of the step free energy, the major component of $\beta(\theta)$ at lower temperatures when the islands are noncircular. Thus, contrary to a proposed method of data analysis,[21] one cannot regenerate $\beta(\theta)$ from $\widetilde{\beta}(\theta)$ by fitting the stiffness to a simple functional form and then integrating twice. In this framework, the linear coefficients of $\cos\theta$ and $\sin\theta$ can be viewed as the two integration constants associated with integrating a second-order differential equation.[22]

C. LOS on fcc{111} has six-fold symmetry

1. General argument

Another important result is that the leading term in the stiffness at low temperature has the full symmetry of the 2D net of binding sites rather than the possibly lower symmetry associated with the full lattice. Specifically, for the present problem of the {111} face of an fcc crystal, the stiffness $\widetilde{\beta}(\theta)$ to lowest order has the full six-fold symmetry of the top layer rather than the three-fold symmetry due to symmetry breaking by the second layer. In contrast, the step energy of B steps ({111} microfacets) differs from that of A-steps

({100} microfacets), leading to islands with the shape of equiangular hexagons with rounded corners, but with sides of alternating lengths (i.e., *ABABAB*).

To see the origin of the six-fold symmetry of the stiffness, suppose without loss of generality that steps in the X' direction have energy E_A per lattice spacing, so that those in the Y' direction have energy E_B. Furthermore, we must make the crucial assumption that any corner energy is negligible. Then all shortest paths to (M', N') have the same energy $M'E_A + N'E_B$, with degeneracy still $g_{M',N'}(0)$. Thus, the free energy is $M'E_A + N'E_B - k_B T \ln g_{M',N'}(0)$, while that of its mirror point (through the line at $\theta = 30°$) is $N'E_A + M'E_B - k_B T \ln g_{N',M'}(0)$. The crux of the proof is that $g_{N',M'}(0) = g_{M',N'}(0)$. Thus, while the free energies at the pair of mirror points differ, the energy parts are obliterated when the stiffness is computed (since M' and N' are linear combinations of $\cos \theta$ and $\sin \theta$), leaving just the contribution from the entropies, which are the same to lowest order.

2. Orientation-dependent three-atom interaction

Within lattice-gas models with only pair interactions, there is no obvious way to distinguish *A* and *B* steps; the minimalist way to obtain different step energies for *A* and *B* steps within the lattice-gas model is to invoke a nonpairwise three-site "trio" interaction associated with three (occupied) sites forming an equilateral triangle with NN sides (See Fig. 5). In contrast to the ones considered heretofore,[23,24] these trio interactions must be *orientation dependent*: If the triangle points in one direction (say up), the interaction energy has a different value than if it points in the opposite (down) direction. Alternatively, one can separate out the average of these two values as an ordinary trio energy with full 6-fold symmetry (the main effect of which presumably is to renormalize the NN interaction[9]); then we can write the new contribution as an *antisymmetric* term which changes sign with each rotation of the triangle by $\pi/3$. The contributions from such a symmetry-breaking interaction would cancel in the interior of an island (in the 2D bulk), but would distinguish *A* and *B* edges. Specifically, each side of the equilateral triangle is associated with a link, so that $1/3$ of its strength can be attributed to each. Each link has a triangle on both sides, one of each orientation. Hence, the difference between the energy per $a_\parallel$ of *A* and *B* steps is $1/3$ the difference between the trio interactions in the two opposite orientations.

For the ground-state, minimum-number-of-links configurations, such a term will not lift the degeneracy since each configuration has the same (1) number of horizontal (X') links, (2) number of right-tilted diagonal links (Y'), and (3) *difference* between the number of convex and concave "kinks" (i.e., bends). Since this statement is not true for higher-energy configurations, the six-fold symmetry is not preserved at higher orders. Nonetheless, at low T it should be a decent approximation for the stiffness (much better than for the island shape).

Thus, our result that the breaking of six-fold symmetry on an fcc {111} is much smaller for the stiffness than for the free energy—is more general than the nearest-neighbor lattice gas model which underlies Eqs. (9) and (10) and the resulting Eq. (18) derived below. We reemphasize that the necessary
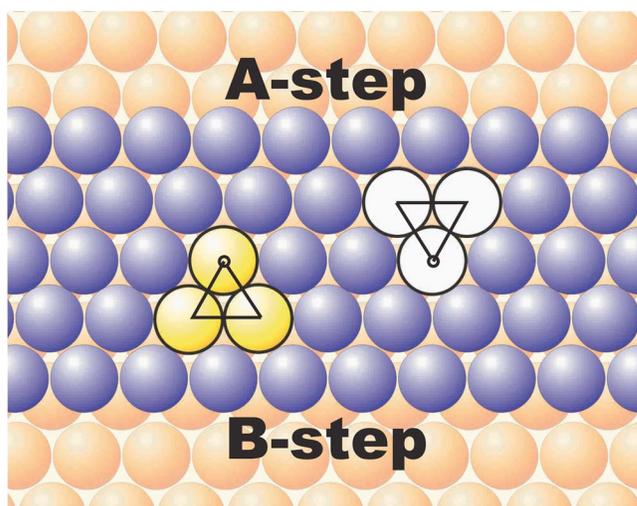

FIG. 5. (Color online) Illustration of A and B steps on fcc {111} surfaces and how orientation-dependent NN equilateral triangles can, within the lattice-gas framework, account for their energy difference—an asymmetry for which one cannot account with just pair interactions. A horizontal link on the A step edge of the [blue] partial overlayer will contribute to a white downward-pointing trio (three-atom, non-pairwise) interaction but not to a light-gray [yellow online] upward-pointing trio. Similarly, a horizontal link on a B step contributes to an upward-pointing but not a downward-pointing trio. As discussed in the text, in this simple picture the energy of an A step per link exceeds that of a B step by 1/3 the energy that a down trio exceeds an up trio. Other trios may also contribute to the asymmetry, most notably from obtuse isosceles triangle configurations with two NN sides and one NNN side.

assumptions are (1) that the orientational dependence of the step energy be just a linear combination of $\sin \theta$ and $\cos \theta$ and (2) that no interaction break the degeneracy of the shortest path corresponding to orientation θ. As above, for angles near close-packed directions, the higher-order terms become important at lower temperatures than for general directions. This feature is illustrated in Fig. 2, and its associated formalism is given in Appendixes A and C.

IV. COMPARISON TO EXPERIMENT

In Fig. 6 we compare Eq. (18) to measurements on Cu{111} and Ag{111}. The experimental data were derived from the equilibrium shape of 2D islands using the method described in Ref. 6. The solid black line corresponds to Eq. (18), while the thick dashed blue line corresponds to the average of the experimental measurements. Equation (18) captures the overall trend and is satisfactory at most angles and temperatures. As expected, Eq. (18) somewhat overestimates $\tilde{\beta}$ near $\theta = 0°$ (since the $T = 0$ singularity remains). Furthermore, near $\theta = 30°$ Eq. (18) somewhat underestimates the experimental $\tilde{\beta}$, but only by a factor of 1/6 for Cu{111} and 1/4 for Ag{111}. This is in striking contrast to the analogous NN theory for Cu{001} near 45°, which understimates $\tilde{\beta}$ by a factor of 4. Finally, notice there is no clear temperature dependence in the measured data. This is further evidence that
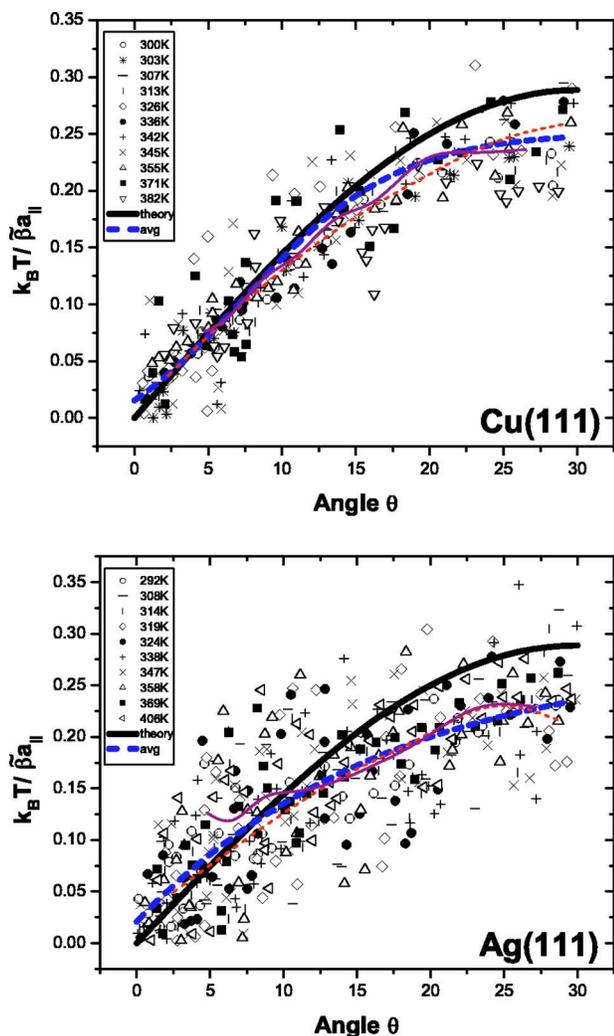
FIG. 6. (Color online) A comparison between Eq. (18) and experiments on Cu and Ag{111}. Equation (18) appears as a solid black line, while the average of the experimental data is a thick dashed blue line. The agreement is reasonable at all angles. In either case the thin dashed red line is a (smoothed) average of the data for the given angle while the thin solid purple line corresponds to the angle mirror-reflected through a radial at 30°, i.e., at $60° - \theta$.

$\tilde{\beta}/k_B T$ is a constant at low temperatures, as Eq. (18) suggests.

The agreement between theory and experiment is a pleasant surprise considering analogous comparisons made for Cu{001} (Ref. 6) found $\tilde{\beta}$ to be 4 times as large as the theoretical value at large angles (near $\theta = 45°$). It was later shown[7–9] that this discrepancy could be partially accounted for by considering next-nearest-neighbor (NNN) interactions (or right-triangle trio interactions, which turn out to affect $\tilde{\beta}$ at low temperatures in the same way). Clearly, the success of Eq. (18) suggests that these interactions are less relevant for {111} surfaces. This is reasonable because the ratio of NNN distance to NN distance is smaller by a factor of $\sqrt{2/3}$ on a triangular lattice compared to on a square lattice. Furthermore, in the close-packed direction ($\theta = 0°$), for every broken NN bond there are only one-and-one-half broken NNN

bonds on a triangular lattice, compared to two broken NNN bonds on a square lattice. These simple arguments help explain why NNN interactions may increase $\tilde{\beta}$ by only 20% to 30% on Cu/Ag{111}, as opposed to 400% on Cu{001} surfaces.

V. CONCLUDING DISCUSSION

By generalizing the low-temperature expansion of the nearest-neighbor square lattice-gas (Ising) model to a triangular lattice, we have found a remarkably simple formula for the orientation dependence of the {111} surface step stiffness. This formula, unlike its square lattice analog, fits experimental data well at general angles, suggesting that NNN interactions are relatively unimportant on {111} surfaces.

To corroborate this picture and explain the success of Eq. (18), we are currently using the VASP package[25] to perform first-principle calculations. In particular, we are examining the ratio of the NNN to NN interaction strength. Preliminary results[26] suggest that this ratio is roughly an order of magnitude smaller on Cu{111} than on Cu{001}, and essentially indistinguishable from zero. This tentative finding is consistent with expectations from the semiempirical embedded atom method, which predicts that indirect interactions are insignificant/negligible between atoms sharing no common substrate atoms.[24] We are also calculating the difference in trio interactions between oppositely oriented triangle configurations.

We expect that our formula, as well as the general six-fold symmetry of the stiffness (except in close-packed directions), should be broadly applicable to systems in which multisite or corner energies are small and for which the bond energies are considerably higher than the measurement temperature. Studies which ignore the three-fold symmetry breaking on metallic fcc {111} substrates, such as a recent investigation of nanoisland fluctuations on Pb{111},[27] should be good representations. Many recent investigations[29,30] focus on the larger asymmetry of the kinetic coefficient,[31] taking the stiffness to be isotropic. In such cases, this stiffness should not be characterized by its value in close-packed directions.

ACKNOWLEDGMENTS

APPENDIX A: LEADING TERM IN LOW-TEMPERATURE EXPANSION

1. Review of results for square lattice

In this appendix we discuss the lowest-order correction to the ground state entropy of the step running from the origin

to an arbitrary particular point. First we review results for a square lattice. We can rewrite Eq. (2) as

$$Z_\theta = g_{M,N}(0)e^{-E_0/kT}\left(1 + \frac{g_{M,N}(1)}{g_{M,N}(0)}e^{-\Delta E/kT} + \cdots\right). \quad \text{(A1)}$$

Then, assuming the exponential is small, we have

$$F \approx E_0 - k_B T\left(\ln[g_{M,N}(0)] + \frac{g_{M,N}(1)}{g_{M,N}(0)}e^{-2\varepsilon/k_B T}\right). \quad \text{(A2)}$$

A combinatorial analysis[3,11,28] shows that

$$g_{M,N}(1) = \binom{M+N}{M-1}(M+1) + \binom{M+N}{N-1}(N+1). \quad \text{(A3)}$$

Then Eq. (4) generalizes to

$$F \approx E_0 - k_B T\Bigg((M+N)\ln(M+N) - M\ln M - N\ln N$$
$$+ e^{-2\varepsilon/k_B T}\frac{M^3+N^3}{MN}\Bigg). \quad \text{(A4)}$$

2. Results for triangular lattice

For the triangular lattice we find important differences from the square lattice for the higher-order terms. Specifically, we consider how $g(1)$ changes. In contrast to $g(0)$, we cannot simply replace M and N with M' and N'. There is no one-to-one correspondence between paths of energy E_1 on a square lattice and those of energy E_1^Δ on a triangular lattice. This failed correspondence for higher terms follows from the observation that E_1^Δ configurations are only one link longer than E_0^Δ steps, whereas E_1 configurations are two links longer than E_0 steps, $E_{n+1}^\Delta - E_n^\Delta \equiv \Delta E^\Delta = \varepsilon$, or

$$E_n^\Delta = \varepsilon\left(\frac{2N}{\sqrt{3}} + 2M + n\right), \quad n = 0,1,2,\dots. \quad \text{(A5)}$$

Hence, we require a separate combinatorial analysis.

We imagine a step of energy E_1 in the first sextant. Such a step (see Fig. 7) will have either (1) $(M'+1)$ links oriented at $0°$ (denoted "X links"), $(N'-1)$ links oriented at $60°$ (denoted "Y links"), and one link oriented at $120°$ (denoted "Υ links"), or (2) $(M'-1)$ links oriented at $0°$, $(N'+1)$ links oriented at $60°$, and one link oriented at $-60°$. In the first case, the problem can be reworded as follows: how many ways to arrange an $(M'+N'+1)$-lettered word with $(M'+1)X$'s, $(N'-1)Y$'s, and one Υ. In the second case, the problem is the same, only with M and N switched. Thus, the solution of this traditional combinatorial problem gives the total number of next-to-shortest paths $g^\Delta(1)$,

$$g^\Delta(1) = \binom{M'+N'+1}{M'+1}N' + \binom{M'+N'+1}{N'+1}M'. \quad \text{(A6)}$$

With $g^\Delta(0/1)$ and E_n^Δ in hand, we can write the low-temperature partition function expansion for a triangular lattice. Using Eq. (3) and expanding the logarithm as in Eq. (28), we have
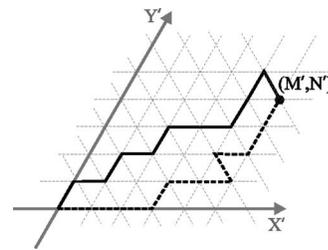

FIG. 7. Two equivalent steps having energy E_1^Δ. The dashed step contains $(M'+1)$ X links, $(N'-1)$ Y links, and one Υ link, while the solid step contains $(M'-1)$ X links, $(N'+1)$ Y links, and one Υ link.

$$F \approx E_0^\Delta - k_B T\left(\ln[g(0)] + \frac{g^\Delta(1)}{g(0)}e^{-\Delta E^\Delta/k_B T}\right). \quad \text{(A7)}$$

Taking the thermodynamic limit $(M',N' \gg 1)$ and using Stirling's approximation gives

$$F \approx E_0^\Delta - k_B T\Bigg((M'+N')\ln(M'+N') - M'\ln M' - N'\ln N'$$
$$+ e^{-\varepsilon/k_B T}\frac{M'^3+N'^3+M'N'^2+N'M'^2}{M'N'}\Bigg). \quad \text{(A8)}$$

The pair of cross factors in the last coefficient are absent in Eq. (A4) for the square lattice.

The correction term becomes non-negligible when the final term in Eq. (A8) becomes of order unity. At low T this occurs only near close-packed directions, so for small values of θ. In this regime, to lowest order in θ, $N' = (2L/\sqrt{3})\sin\theta \to 2L\theta/\sqrt{3}$ and $M' = L\cos\theta - N'/2 \to L$. Then the critical value of θ is

$$\theta_c^{(\beta)} \approx \frac{\sqrt{3}}{2}e^{-\varepsilon/k_B T} = \frac{\sqrt{3}}{2}z^{1/2}. \quad \text{(A9)}$$

Specifically, based on Eq. (A9) and using $\varepsilon \approx 0.12$ eV for Cu{111}, we find that $\theta_c^{(\beta)}$ is $0.353°$, $3.18°$, and $5.51°$ for T/T_c of 1/9, 1/5, and 1/4, respectively. From Fig. 3, this criterion turns out to underestimate the values for θ_c obtained in Sec. II D, mainly because Eq. (A9) was derived from an expression for $\beta(\theta)$ instead of $\tilde{\beta}(\theta)$ (which should depend more sensitively on θ).

APPENDIX B: EXACT FORMULAS FOR LINE TENSION AND STIFFNESS IN MIRROR DIRECTIONS

1. General results for all orientations

In this appendix, we derive Eqs. (22)–(25) for the mirror-line directions $\theta = 0°$ and $\theta = 30°$ from Zia's implicit exact solution.[5]

To begin, because $\tilde{\beta} = \beta + \beta''$ (where the prime represents differentiation with respect to θ), it follows from Eq. (19) that
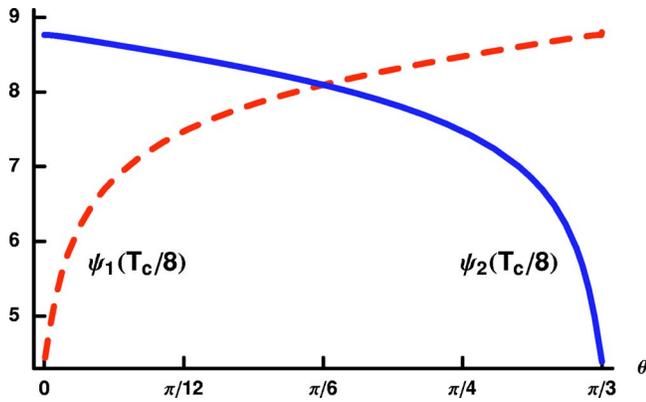
FIG. 8. (Color online) Numerical evaluation of ψ_1 (dashed red curve) and ψ_2 (solid blue curve) as functions of angles at temperature $T_c/8$ equivalent to room temperature for the experimental systems Cu and Ag {111}. Note the linear behavior near one limit and the divergent slope at the other, the factor-of-2 difference at either limit, and the symmetry about $\pi/6$. At higher temperatures the curves are qualitatively similar but progressively smaller in magnitude.

$$\frac{\tilde{\beta} a_\parallel}{k_B T} = 2\eta_0' \psi_1' + 2\eta_-' \psi_2' + \eta_0 \psi_1'' + \eta_- \psi_2''. \quad (B1)$$

We can simplify Eq. (B1) by finding relationships between the various derivatives of the ψ's. Differentiating Eq. (21) with respect to θ, regrouping, and using Eq. (20), we get

$$\psi_1' \eta_0 + \psi_2' \eta_- = 0. \quad (B2)$$

Differentiating again yields

$$\psi_1'' \eta_0 + \psi_2'' \eta_- + \psi_1' \eta_0' + \psi_2' \eta_-' = 0. \quad (B3)$$

Using Eq. (B3), we rewrite the last part of Eq. (B1) (containing ψ_1'' and ψ_2'') in terms of just ψ_1' and ψ_2'. Then, using Eq. (B2) we eliminate ψ_2' in favor of ψ_1'. We are then left with an equation relating $\tilde{\beta}$ to only ψ_1',

$$\frac{\tilde{\beta} a_\parallel}{k_B T} = \left(\eta_0' - \eta_-' \frac{\eta_0}{\eta_-}\right)\psi_1' = \frac{2\psi_1'}{\sqrt{3}\cos\theta - \sin\theta}. \quad (B4)$$

For general angle, we must evaluate ψ_1' numerically. (To get some understanding of the behavior of ψ_1 and ψ_2, see Fig. 8, which shows their numerical evaluation for temperature $T_c/8$. However, for the two high-symmetry directions we can obtain analytic results that allow us [with the aid of Eq. (19) for β] to write explicit expressions for $\tilde{\beta}$, as presented in the next two sections.

2. Results for $\theta=0°$

At $\theta=0°$, Eq. (19) reduces to

$$\frac{\beta a_\parallel}{k_B T} = \psi_2(0), \quad (B5)$$

assuming that $\psi_1(0)$ is finite. Furthermore, near $\theta=0°$, Eq. (20) can be inverted and the sinh's combined to get

$$\frac{\sinh(\psi_1 - \frac{1}{2}\psi_2)\cosh(\frac{1}{2}\psi_2)}{\sinh(\psi_2 - \frac{1}{2}\psi_1)\cosh(\frac{1}{2}\psi_1)} = \frac{2}{\sqrt{3}}\theta. \quad (B6)$$

For Eq. (B6) to hold at $\theta=0°$,

$$\psi_2(0) = 2\psi_1(0). \quad (B7)$$

Equation (21) therefore becomes

$$2\cosh\psi_1(0) + \cosh[2\psi_1(0)] = f. \quad (B8)$$

Solving this for $\cosh\psi_1(0)$ and taking the positive root, we find

$$\cosh\psi_1(0) = \cosh\left[\tfrac{1}{2}\psi_2(0)\right] = \tfrac{1}{2}(-1 + \sqrt{3 + 2f}), \quad (B9)$$

consistent with the assumption of finite $\psi_1(0)$. Solving for $\psi_2(0)$ and combining with Eq. (B5) yields Eq. (22).

Correspondingly for $\tilde{\beta}$, at $\theta=0°$, Eq. (B4) becomes

$$\frac{\tilde{\beta}(0)a_\parallel}{k_B T} = \frac{2}{\sqrt{3}}\psi_1'(0), \quad (B10)$$

while Eq. (B2) becomes

$$\psi_2'(0) = 0, \quad (B11)$$

provided $\psi_1'(0)$ is finite. We obtain $\psi_1'(0)$ by differentiating Eq. (B6) with respect to θ and then setting $\theta=0°$ so that Eqs. (B7) and (B11) apply. This gives

$$\psi_1'(0) = \frac{1}{\sqrt{3}}\tanh\psi_1(0)[1 + 2\cosh\psi_1(0)]. \quad (B12)$$

By combining this with Eq. (B9) for $\cosh\psi_1(0)$, we see that $\psi_1'(0)$ is indeed finite, as we earlier assumed. Thus, Eq. (B10) becomes Eq. (23), as desired.

3. Results for $\theta=30°$

At $\theta=30°=\pi/6$, Eq. (19) becomes

$$\frac{\beta(\pi/6)a_\parallel}{k_B T} = \frac{1}{\sqrt{3}}[\psi_1(\pi/6) + \psi_2'(\pi/6)]. \quad (B13)$$

Furthermore, near $\theta=\pi/6$, $\eta_0/\eta_- \approx 1 + 2\sqrt{3}\Delta\theta$, where $\Delta\theta \equiv \theta - \pi/6$. Inverting Eq. (20) we therefore have

$$\frac{\sinh\psi_1 + \sinh(\psi_1 - \psi_2)}{\sinh\psi_2 - \sinh(\psi_1 - \psi_2)} \approx 1 + 2\sqrt{3}\Delta\theta. \quad (B14)$$

By inspection, at $\theta=\pi/6(\Delta\theta=0)$, one solution to this equation is just

$$\psi_2(\pi/6) = \psi_1(\pi/6). \quad (B15)$$

Plugging this result into Eq. (21) and solving for $\psi_2(\pi/6)$ gives

$$\cosh\psi_2(\pi/6) = \frac{f-1}{2}. \quad (B16)$$

Combining this with Eq. (B13) [where we now know $\psi_1(\pi/6) = \psi_2(\pi/6)$] results in Eq. (24).

As for $\widetilde{\beta}$, at $\theta = \pi/6$, Eq. (B4) becomes

$$\frac{\widetilde{\beta} a_{\parallel}}{k_B T} = 2\psi_1'(\pi/6), \tag{B17}$$

while Eq. (B2) becomes

$$\psi_1'(\pi/6) = -\psi_2'(\pi/6). \tag{B18}$$

Like before, we can find $\psi_1'(\pi/6)$ by differentiating Eq. (B14) with respect to θ. Taking the result and setting $\theta = \pi/6$, so that Eqs. (B15) and (B18) apply, gives

$$\psi_1'(\pi/6) = \frac{\sqrt{3} \sinh \psi_1}{\cosh \psi_1 + 2}. \tag{B19}$$

Finally, we combine this result with Eq. (B16) for $\cosh \psi_2(\pi/6) = \cosh \psi_1(\pi/6)$ and Eq. (B17), to get Eq. (25), as desired.

APPENDIX C: REDERIVATION OF EQ. (18) FROM EXACT SOLUTION

In this appendix, we re-derive Eq. (18) directly from the exact solution for $\beta(\theta)$ given in Eqs. (20) and (21). To do so, we just assume $\cosh \psi_2 \gg \eta_-/\eta_0$ (remember that η_-/η_0 decreases from ∞ at $\theta = 0°$ to 1 at $\theta = 30°$, so that, between these angles, this condition also implies that $\cosh \psi_2 \gg 1$). In this case, Eq. (20) can be solved to give

$$\cosh \psi_1 \approx \frac{\eta_0}{\eta_-} \cosh \psi_2. \tag{C1}$$

Thus, if $\cosh \psi_2 \gg \eta_-/\eta_0 > 1$, then $\cosh \psi_1 \gg 1$. We show here that these assumptions for $\cosh \psi_{1,2}$, together with the low-temperature replacement of $f(z)$ by $1/(2z)$ in Eq. (21), are enough to derive Eq. (18).

When $\cosh \psi_{1,2} \gg 1$, then $\cosh \psi_{1,2} \approx \sinh \psi_{1,2} \approx e^{\psi_{1,2}}/2$. With these approximations, Eqs. (20) and (21) become remarkably simple,

$$e^{\psi_1} + e^{\psi_2} = 2f(z), \tag{C2}$$

$$e^{\psi_2} = \frac{\eta_-}{\eta_0} e^{\psi_1}. \tag{C3}$$

Solving this pair of equations for e^{ψ_1} and e^{ψ_2} gives

$$e^{\psi_1} = \frac{2f(z)\eta_0}{\eta_0 + \eta_-}, \quad e^{\psi_2} = \frac{2f(z)\eta_-}{\eta_0 + \eta_-}. \tag{C4}$$

If we then replace $f(z)$ by its low-temperature limit, $1/(2z)$, Eq. (19) becomes

$$\frac{\beta a_{\parallel}}{k_B T} = \eta_0 \ln\left(\frac{\eta_0}{z(\eta_0 + \eta_-)}\right) + \eta_- \ln\left(\frac{\eta_-}{z(\eta_0 + \eta_-)}\right). \tag{C5}$$

By noting $\eta_0 + \eta_- = \eta_+$, and using the definition for z, Eq. (C5) can be easily simplified to Eq. (9), from which Eq. (18) for $\widetilde{\beta}$ was derived.

By deriving the approximation given in Eq. (9) [and thus Eq. (18)] in this way, we can determine when the approximation becomes invalid. Specifically, we require $\cosh \psi_{1,2} \gg 1$. As we showed, the more restrictive of these inequalities is the one involving $\cosh \psi_1$, since $\cosh \psi_1$ is necessarily smaller than $\cosh \psi_2$ in the first sextant by a factor of η_0/η_- (which is less than 1). Thus, the main assumption is $\cosh \psi_1 \gg 1$, which, from Eq. (C4), is just

$$\frac{2f(z)\eta_0}{\eta_0 + \eta_-} \gg 1. \tag{C6}$$

The solution to this inequality, which we call θ_2, is given by the following inequality:

$$\cot \theta_2 \ll \frac{4f - 1}{\sqrt{3}}. \tag{C7}$$

Because $\cot \theta$ decreases from ∞ at $\theta = 0$ to $1/\sqrt{3}$ at $\theta = \pi/6$, we know that angles in the first sextant that are greater than θ_2 will also satisfy the inequality in Eq. (C7). Thus, Eqs. (9) and (18) are valid in the first sextant at all angles above θ_2.

*Electronic address: tjs@glue.umd.edu; http://www2.physics.umd.edu/~tjs

†Corresponding author, Electronic address: einstein@umd.edu; http://www2.physics.umd.edu/~einstein/

[1] H.-C. Jeong and E. D. Williams, Surf. Sci. Rep. **34**, 171 (1999).

[2] D. B. Abraham and P. Reed, J. Phys. A **10**, L8121 (1977).

[3] C. Rottman and M. Wortis, Phys. Rev. B **24**, 6274 (1981).

[4] J. E. Avron, H. van Beijeren, L. S. Schulman, and R. K. P. Zia, J. Phys. A **15**, L81 (1982); R. K. P. Zia and J. E. Avron, Phys. Rev. B **25**, 2042 (1982).

[5] R. K. P. Zia, J. Stat. Phys. **45**, 801 (1986).

[6] S. Dieluweit, H. Ibach, M. Giesen, and T. L. Einstein, Phys. Rev. B **67**, 121410(R) (2003).

[7] R. Van Moere, H. J. W. Zandvliet, and B. Poelsema, Phys. Rev. B **67**, 193407 (2003).

[8] H. J. W. Zandvliet, R. Van Moere, and B. Poelsema, Phys. Rev. B **68**, 073404 (2003).

[9] T. J. Stasevich, T. L. Einstein, R. K. P. Zia, M. Giesen, H. Ibach, and F. Szalma, Phys. Rev. B **70**, 245404 (2004).

[10] M. Giesen, C. Steimer, and H. Ibach, Surf. Sci. **471**, 80 (2001).

[11] J. W. Cahn and R. Kikuchi, J. Phys. Chem. Solids **20**, 94 (1961).

[12] In deriving the equivalent of our Eq. (9) for honeycomb lattices, N. Akutsu, J. Phys. Soc. Jpn. **61**, 477 (1992) noted that what we call $\eta_\pm(\theta)$ can be written $(2/\sqrt{3})\sin(\theta \pm \pi/3)$.

[13] This simple equivalency does not hold for stepped surfaces in an electrochemical system, where the electrode potential ϕ is fixed rather than the surface charge density conjugate to ϕ. H. Ibach and W. Schmickler, Phys. Rev. Lett. **91**, 016106 (2003). Other noteworthy subtleties in the free energy are discussed by N. Akutsu and Y. Akutsu, J. Phys. Soc. Jpn. **64**, 736 (1995).

[14] G. Schulze Icking-Konert, M. Giesen, and H. Ibach, Phys. Rev. Lett. **83**, 3880 (1999).

[15] G. H. Wannier, Rev. Mod. Phys. **17**, 50 (1945).

[16] The calculation can be facilitated by writing $\eta_i \equiv a_i \cos \theta + b_i \sin \theta$ and then using Eq. (14) to show $\tilde{s}_i = [(b_i^2 - a_i^2)(\cos^2 \theta - \sin^2 \theta) - 4a_i b_i \sin \theta \cos \theta]/[a_i \cos \theta + b_i \sin \theta]$.

[17] Equation (21) bypasses several intermediate quantities that are important for Zia's (Ref. 5) general treatment but cumbersome here. Our ψ_2 has the opposite sign from Zia's, and our angle θ—which vanishes for close-packed step orientations—differs by 30° from his. Note also that interchanging ψ_1 and ψ_2 on the left-hand side of Eq. (20) inverts the left-hand side, from which it is easy to see that $\beta(\theta)$ of Eq. (19) is symmetric about $\theta = 30°$. The left-hand side of Eq. (21) is obviously invariant under the interchange of ψ_1 and ψ_2.

[18] N. Akutsu and Y. Akutsu, J. Phys.: Condens. Matter **11**, 6635 (1999).

[19] In Eqs. (4.30)–(4.33) of Ref. 18, their W corresponds to our z^2 and their angles, like Zia's (Refs. 5 and 17) differ from ours so that their $\pi/2$ is our 0 and their 0 is our $\pi/6$.

[20] C. Herring, Phys. Rev. **82**, 87 (1951).

[21] M. Ondrejcek, W. Swiech, C. S. Durfee, and C. P. Flynn, Surf. Sci. **541**, 31 (2003).

[22] J. Krug (private communication).

[23] T. L. Einstein, Langmuir **7**, 2520 (1991); G. Ehrlich and F. Watanabe, *ibid.* **7**, 2555 (1991); B. N. J. Persson, Surf. Sci. Rep. **15**, 1 (1992).

[24] T. L. Einstein, in *Handbook of Surface Science*, edited by W. N. Unertl (Elsevier Science B. V., Amsterdam, 1996), Vol. 1, Chap. 11.

[25] G. Kresse and J. Hafner, Phys. Rev. B **47**, R558 (1993); **49**, 14251 (1994); Comput. Mater. Sci. **6**, 15 (1996); Phys. Rev. B **54**, 11169 (1996).

[26] T. J. Stasevich, T. L. Einstein, and S. Stolbov (in preparation).

[27] F. Szalma, Hailu Gebremariam, and T. L. Einstein, Phys. Rev. B **71**, 035422 (2005).

[28] There appears to be a pair of sign or letter typographic errors in Eq. (11) of Ref. 3.

[29] G. Danker, O. Pierre-Louis, K. Kassner, and C. Misbah, Phys. Rev. E **68**, 020601(R) (2003).

[30] P. Kuhn and J. Krug, in *Multiscale Modeling of Epitaxial Growth*, edited by A. Voigt, (Birkhäuser, Basel, in press), cond-mat/0405068.

[31] M. Giesen and S. Dieluweit, J. Mol. Catal. A: Chem. **216**, 263 (2004).